AIP | Journal of Applied Physics

μ-Raman spectroscopy characterization of LiNbO3 femtosecond laser written waveguides

M. R. Tejerina, D. Jaque, and G. A. Torchia

Citation: J. Appl. Phys. **112**, 123108 (2012); doi: 10.1063/1.4769869
View online: http://dx.doi.org/10.1063/1.4769869
View Table of Contents: http://jap.aip.org/resource/1/JAPIAU/v112/i12
Published by the American Institute of Physics.

Related Articles

Efficient coupler between silicon photonic and metal-insulator-silicon-metal plasmonic waveguides
Appl. Phys. Lett. 101, 251117 (2012)

Experimental demonstration of a four-port photonic crystal cross-waveguide structure
Appl. Phys. Lett. 101, 251113 (2012)

Experimental realization of bending waveguide using anisotropic zero-index materials
Appl. Phys. Lett. 101, 253513 (2012)

Mode latching and self tuning of whispering gallery modes in a stand-alone silica microsphere
Appl. Phys. Lett. 101, 251105 (2012)

Ultralow VπL values in suspended quantum well waveguides
Appl. Phys. Lett. 101, 241111 (2012)

Additional information on J. Appl. Phys.

Journal Homepage: http://jap.aip.org/
Journal Information: http://jap.aip.org/about/about_the_journal
Top downloads: http://jap.aip.org/features/most_downloaded
Information for Authors: http://jap.aip.org/authors

ADVERTISEMENT

AIP Advances
Now Indexed in Thomson Reuters Databases
Explore AIP's open access journal:
- Rapid publication
- Article-level metrics
- Post-publication rating and commenting

Downloaded 21 Dec 2012 to 163.10.0.68. Redistribution subject to AIP license or copyright; see http://jap.aip.org/about/rights_and_permissions

μ-Raman spectroscopy characterization of $LiNbO_3$ femtosecond laser written waveguides

M. R. Tejerina,[1] D. Jaque,[2] and G. A. Torchia[1,a)]
[1]*Centro de Investigaciones Ópticas, CONICET-CIC, Cno. Centenario y 506, M.B.Gonnet, 1897 Pcia. Buenos Aires, Argentina*
[2]*Departamento de Física de Materiales, GIEL, Facultad de Ciencias, Universidad Autónoma de Madrid, Campus de Cantoblanco, Madrid 28049, Spain*

(Received 6 June 2012; accepted 19 November 2012; published online 21 December 2012)

In this paper, we present an iterative method which merges experimental μ-Raman measurements and numerical simulations to describe femtosecond written waveguides in $LiNbO_3$ crystals. This method is based on the deformation potential theory, and uses the finite element method to analyze elastic deformations after femtosecond laser micro-explosions in x-cut Mg:$LiNbO_3$ crystals. The resultant strain and refractive index field after laser interaction were estimated and yielded similar values to those obtained in other works. The $LiNbO_3$ Raman deformation potential constants were also estimated in this work. © *2012 American Institute of Physics*. [http://dx.doi.org/10.1063/1.4769869]

I. INTRODUCTION

Ultra-short pulse (of hundreds of femtoseconds) laser writing has emerged in the last decade as an important tool for optical circuit fabrication. This method can be applied in an unlimited number of optical materials. The non-linear absorption as a consequence of there being many infrared photons in the focused region is the key to obtaining a suitable modification. In this sense, a large number of successful integrated guiding structures have been reported.[1,2]

Femtosecond laser written waveguides have different optical properties according to the processing parameters employed. Because of the complexity of the physical phenomena, these parameters have been analyzed by several authors using empirical methods.[3–6] Therefore, the processing parameters which can be used to generate a permanent waveguide are well-known, but the refractive index field of these waveguides has not been sufficiently studied.

On the basis of what is said above, femtosecond laser pulse interaction with transparent materials has at least two important aspects which are worth studying. One of these is the resulting strain field and, thus, the refractive index variation field, and the other is the non-thermodynamic expansion characteristics after femtosecond laser pulse interaction.

In the first of these research fields, this work provides an approximated quantitative description of the residual refractive index and residual strain field of femtosecond laser waveguides. This is the result of experimental μ-Raman measurements and a self-developed finite-element code. By this procedure, the Nd:MgO:$LiNbO_3$ piezo-spectroscopic constants were also estimated in this work.

In the second of these research fields, the non-thermodynamic expansion process and the material phase modification generated from the interaction of femtosecond laser pulses with a transparent medium can be studied using the method presented in this paper.

Not much information is known about this phenomenon because it has many special characteristics. One of these is that the plasma is generated inside a material which has a high elastic constant. This generates a very high pressure if the plasma "tries" to expand, so the situation is very different from that existing in normal atmospheric conditions and it seems to be very difficult to reproduce it using other methods.[7–15]

It is estimated that the phenomenon called "micro-explosion" goes through the following steps:[16] nonlinear absorption, ionization, and reverse sublimation. According to previous works, inside the directly modified region during the expansion process pressures and temperatures near 1000 GPa and 10^6 K, respectively, are achieved. These values depend on the physical properties of the material and the laser processing conditions.[16–20]

Associated with this research field, this work analyzes geometric characteristics of the volume change generated in the irradiated material after micro-expansion. This contribution is related to the basic physics of material-laser interaction.

Furthermore, studies of residual stresses at the micro-scale using Raman spectroscopy can be divided into two important groups. The first relates to materials used in micro-electronics and micro electro-mechanical (MEMS) manufacturing,[21–32] and the other relates to photonic materials.[33–36] These photonic materials are used as bulk material for the generation of optical and electro-optical circuits.

The rapidly increasing number of electronic technology requirements has been the main reason for there being far more studies in the first group than in the second one.

This work can be classified as falling within the second topic because it deals with residual strain analysis in Mg:Nd:$LiNbO_3$ crystals, and this material is used to generate photonic structures.

II. THEORETICAL FRAMEWORK: DEFORMATION POTENTIAL THEORY AND NUMERICAL MODEL

A. Deformation potential theory

Deformation potential theory relates the spectral shifts of Raman optical phonons to mechanical deformation. It associates a potential variation V of a crystal with the strain

a)gustavot@ciop.unlp.edu.ar.

 © 2012 American Institute of Physics

Downloaded 21 Dec 2012 to 163.10.0.68. Redistribution subject to AIP license or copyright; see http://jap.aip.org/about/rights_and_permissions

field ε_{ij}. Using a linear approximation, in the presence of deformations the energy variation, ΔE, is represented by[28,33]

$$\Delta E = \sum_{i,j} V_{ij}\varepsilon_{ij} = V_{xx} \times \varepsilon_{xx} + V_{yy} \times \varepsilon_{yy} + V_{zz} \times \varepsilon_{zz} + V_{xy} \times \varepsilon_{xy} + V_{xz} \times \varepsilon_{xz} + V_{yz} \times \varepsilon_{yz}, \quad (1)$$

where V_{ij} represents the deformation potential tensor, and ε_{ij} represents the strain tensor.

Lithium niobate ($LiNbO_3$) belongs to the 3C spatial group and has 3 symmetries of optical phonons (A_1, E_1, and E_2). In this work, only A_1 transverse optical phonons (TOs) were used.

The A_1 phonon Raman matrix and A_1 phonon base functions are[33]

$$A_1\ Raman\_Matrix: \begin{bmatrix} p & 0 & 0 \\ 0 & p & 0 \\ 0 & 0 & q \end{bmatrix}$$
$$A_1 \text{ base functions}: X^2 + Y^2, Z^2. \quad (2)$$

The terms in Eq. (1) can be conveniently grouped as follows:

$$\sum_{i,j} V_{ij} \times \varepsilon_{ij} = \frac{1}{2} \times (V_{xx} + V_{yy}) \times (\varepsilon_{xx} + \varepsilon_{yy}) + V_{zz} \times \varepsilon_{zz} + \frac{1}{2} \times [(V_{xx} - V_{yy}) \times (\varepsilon_{xx} - \varepsilon_{yy}) + (-2V_{xy}) \times (-2\varepsilon_{xy})] + 2 \times V_{yz} \times \varepsilon_{yz} + (-V_{zx}) \times (-\varepsilon_{zx}). \quad (3)$$

Taking into account Eqs. (2) and (3), the Raman phonon energy variation (ΔEA_1) for A_1(TO) can be expressed as a function of strain. This is shown in the following equation:

$$\Delta E_{A1(TO)i} = e_i \times (\varepsilon_{xx} + \varepsilon_{yy}) + f_i \times (\varepsilon_{zz}), \quad (4)$$

where e, f are the A_1 phonon deformation potential constants, and ΔE_{A1} is the A_1 phonon energy variation.

The shear components of the strain tensor (i.e., ε_{xy}, ε_{xz}, ε_{yz}) do not appear in Eq. (4) because the non-diagonal A_1 Raman matrix components are all equal to zero.

As can be seen in Eq. (4), the A_1 deformation potential constants e and f relate the phonon energy shifts to the normal strain field.

To express phonon energy shifts as a function of stress, a material compliance matrix is needed. The $Mg:LiNbO_3$ compliance matrix is

$$\begin{bmatrix} S_{xx} \\ S_{yy} \\ S_{zz} \\ S_{xy} \\ S_{xz} \\ S_{yz} \end{bmatrix} = \begin{bmatrix} C_{11} & C_{12} & C_{13} & C_{14} & 0 & 0 \\ : & C_{11} & C_{13} & -C_{14} & 0 & 0 \\ : & : & C_{33} & 0 & 0 & 0 \\ : & : & 0 & C_{44} & 0 & 0 \\ 0 & 0 & 0 & 0 & C_{55} & C_{56} \\ 0 & 0 & 0 & 0 & : & C_{66} \end{bmatrix} \times \begin{bmatrix} \varepsilon_{xx} \\ \varepsilon_{yy} \\ \varepsilon_{zz} \\ \varepsilon_{xy} \\ \varepsilon_{xz} \\ \varepsilon_{yz} \end{bmatrix}, \quad (5)$$

where ":" means symmetric element.

$C_{11} = 200$ GPa, $C_{22} = 200$ GPa, $C_{33} = 235$ GPa, $C_{12} = 53.3$ GPa, $C_{13} = 67.7$ GPa, $C_{14} = 8.7$ GPa, $C_{44} = 53.5$ GPa, $C_{55} = 53.5$ GPa, $C_{66} = 53.5$ GPa, $C_{56} = 9.7$ GPa

By ordering Eq. (5) and replacing it in Eq. (4), Eq. (6) is obtained

$$\Delta E_{A1} = e' \times (S_{xx} + S_{yy}) + f' \times (S_{zz}), \quad (6)$$

where

$$e' = e \times (C_{11} + C_{12}) + f \times (C_{13}), \quad (7)$$
$$f' = 2 \times eC_{13} + f \times C_{33}. \quad (8)$$

The values of e, f, e', and f' have never, so far as we know, been measured in $LiNbO_3$ crystals.

B. A_1(TO) phonon energy shift due to hydrostatic pressure ($d\omega/dp$)

From Eq. (6), it can easily be deduced that ΔE_{A1} is equal to $2 \times e' + f'$ when the crystal is under hydrostatic pressure. In this special condition, $\Delta E_{A1} = d\omega/dp$, so Eq. (9) is reached,

$$d\omega/dp_i = 2 \times e'_i + f'_i. \quad (9)$$

The values of $d\omega/dp$ for $LiNbO_3$ have been measured experimentally.[37,38] These values were used in the current method to estimate the ellipse expansion geometry in the numerical model.

C. $A_1(TO)_i$ dw/dp_i variation with Mg- and Nd-doping

Neither the value of Mg:$LiNbO_3$ A_1(TO) $d\omega/dp_i$ nor the value of Mg:Nd:$LiNbO_3$ A_1(TO) $d\omega/dp_i$ have been measured experimentally. The Nd:Mg:$LiNbO_3$ Raman spectrum was compared with pure $LiNbO_3$ in the following works.[39–41] In these works, the following information is reported: for the $A_1(TO)_2$ and $A_1(TO)_3$ modes, small energy displacements were detected between doped and undoped $LiNbO_3$, while for the $A_1(TO)_1$ and $A_1(TO)_4$ modes, no energy shift between doped and undoped $LiNbO_3$ was detected.

From the above, we can assume that $LiNbO_3$ A_1(TO) $d\omega/dp_1$ and A_1(TO) $d\omega/dp_4$ do not vary with Nd- and Mg-doping. From this assumption, the $d\omega/dp_1$ and $d\omega/dp_4$ reported in other works[37,38] were used in the current work to estimate the ellipse expansion geometry in the numerical model.

D. Numerical model: Waveguide origin and femtosecond laser pulse residual strain

1. Assumptions/approximations

Some assumptions used in Refs. 7, 42–44 were also used in the current work, while other assumptions were replaced or modified. In this section, each of the assumptions is explained and justified.

a. Residual strain method and photo-elasticity. In the present work, it was assumed that femtosecond laser waveguide residual deformations could be obtained from a

Downloaded 21 Dec 2012 to 163.10.0.68. Redistribution subject to AIP license or copyright; see http://jap.aip.org/about/rights_and_permissions

numerical model, where an ellipse statically expanded within an elastic medium. It was also assumed that the refractive index variation was only due to the residual strain field, by means of the piezo-optic relationship. Both assumptions were used in this work because they had yielded acceptable results in other papers.[7,42–44]

b. Linear elastic deformation. The linear elastic deformation hypothesis was used in the current work because it had yielded good results in previous papers[42–44] and also because of its simplicity. Other more complex models, including plastic deformation, are proposed for future works as we think that this analysis exceeds the scope of the present work.

c. Plane strain ($\varepsilon_{yy}=0$, $\varepsilon_{zy}=0$, $\varepsilon_{yx}=0$). A plane strain assumption has been used in several works,[42–44] with good results. Before using this assumption, we will discuss when it can be applied to anisotropic material deformations.

In plane strain deformation, all deformation components not contained in the selected plane are required to be equal to zero. This simplification is applied to isotropic materials, and requires that the load does not vary in the direction normal to the analyzed plane. For example, it can be used to analyze a cylindrical tube under internal pressure. From a loading and geometric point of view, this example is similar to the problem solved in this work, but when the symmetry of the material is considered, it is not. This is because $LiNbO_3$ is an anisotropic material which normally does not allow plane strain deformation. Not all anisotropic materials allow the plane strain assumption to be made. Although the symmetry of loads corresponds to that necessary for plane strain deformation, unless the material plane of symmetry coincides with the selected plane, plane strain is not possible (e.g., if the selected plane is xz: $\varepsilon_{yy}=0$ but $\varepsilon_{zy}\neq 0$ and $\varepsilon_{yx}\neq 0$).

For anisotropic materials, if the plane of symmetry coincides with the selected plane, the deformation can be decomposed into "in-plane deformation" and "anti-plane deformation," which are uncoupled deformations.[45] In this case, plane strain simplification can be used to determine in-plane deformations. A $LiNbO_3$ crystal does not have a symmetry plane in the analyzed plane (xz), but the value of the compliance matrix element which means that $LiNbO_3$ does not have this symmetry, (C_{14}), is about 70 times smaller than the other matrix elements. Also, it was numerically verified in Ref. 46 that plane strain deformation is an acceptable assumption for the material symmetry and the plane selected in the current work. Taking into account the previous paragraphs, plane strain deformation was conducted in the present work.

d. Nd- doping does not produce changes in the $LiNbO_3$ compliance matrix. According to ultrasonic experiments from previous works,[47–49] the variation in the $LiNbO_3$ compliance matrix due to Mg-doping is low (about 2%). No explicit information was found about the effect of Nd-doping on the compliance matrix. So, taking into account the following information:

- The Nd ion is in a lower ratio (0.3%) than that of the Mg ion (5%) and is situated only in some unitary cells of the crystal structure;[40] and
- There are no reported changes in the $LiNbO_3$ Raman spectrum because of this rare earth doping,[40]

it is assumed that Nd-doping does not affect the $LiNbO_3$ compliance matrix, so the Mg:$LiNbO_3$ compliance matrix, shown in Eq. (5), is used for our numerical simulations.

e. Non-proportional expansion. In others works,[42] for qualitative analysis, it is supposed that the geometries before and after the expansion are proportional to each other. Taking into account the volume change shown in Eq. (10), it is easy to see that under proportional expansion: $\frac{\Delta a}{a}=\frac{\Delta b}{b}$, where a and b are the initial minor and major axis and Δa and Δb are the minor and major radii variations, respectively.

This assumption is not used in a later work,[44] in which the values for $\frac{\Delta a}{a}$ and $\frac{\Delta b}{b}$ to match the waveguides near field experimental results, were not explicitly mentioned.

The volume variation is

$$\frac{\Delta V}{V}=\frac{\Delta a}{a}+\frac{\Delta b}{b}. \tag{10}$$

Considering that the origin of the physical process is a "micro-expansion" and re-solidification of an amorphous material,[44] we infer the following:

- In the elliptical geometry model of the laser-material interaction zone, if the effect of an internal pressure is studied as if it were exerted by a gas, the resulting deformation would be qualitatively different from that produced by a proportional expansion.[46]
- On the other hand, the effect mentioned above could be modified by material re-solidification, which would generally result in a different deformation from that obtained from the application of an internal pressure.

Considering this analysis, we thought it unsuitable to perform a quantitative analysis using the geometrical proportionality assumption, so $\frac{\Delta a}{a}\neq\frac{\Delta b}{b}$ was assumed.

Expansion parameters for lithium niobate under similar conditions have not yet been estimated or measured, although they have been estimated for other materials such as cerium, samarium sulfide, germanium, and bismuth.[50]

As the estimation of the experimental or analytical geometric change which takes place in the explosion process is beyond the scope of this study, the deformation parameters become setting parameters. The expression adopted for them is presented in Eq. (11).

The following statements about the expressions in Eq. (11) must be taken into account:

(i) The expressions are applied to a first quadrant ellipse quarter, so the signs should be appropriately changed for using them in other quadrants.

(ii) The degree of the expressions in Eq. (11) is established at 3 to improve the boundary fit, and the form of them is selected in such a way as to not have discontinuities for $x=0$ and $y=0$ (boundary quadrants) for either the displacements or their derivatives,

$$\begin{aligned}\Delta z_i &= \alpha_1\times z_i+\alpha_2\times {z_i}^2+\alpha_3\times {z_i}^3,\\ \Delta x_i &= \beta_1\times x_i+\beta_2\times {x_i}^2+\beta_3\times {x_i}^3,\end{aligned} \tag{11}$$

Downloaded 21 Dec 2012 to 163.10.0.68. Redistribution subject to AIP license or copyright; see http://jap.aip.org/about/rights_and_permissions

where Δz_i is the i-point x-direction displacement along the ellipse boundary; Δx_i is the i-point y-direction displacement along the ellipse boundary; z_i is the x-coordinate of the i-point; x_i is the y-coordinate of the i-point; and α_i and β_i are setting parameters.

f. Hypothetical expansion of the ellipse. The resultant variation of the refractive index in the filament has been qualitatively used in Refs. 42 and 44, which have been mentioned above, to estimate the volume change produced during expansion. This has been done using the Clausius-Mossotti relation[51] presented in Eq. (12a). In the current work, as stated before, the parameters which define the ellipse area variation are used as setting parameters and they were not set beforehand. However, Eqs. (10) and (12b) were used to estimate initial values of the setting parameters in the present work,

$$\frac{\Delta V}{V} = -\frac{6 \times n}{(n^2+2) \times (n^2-1)} \times \Delta n, \tag{12a}$$

$$\frac{\Delta V}{V} = -0.5 \times \Delta n, \tag{12b}$$

where n is the material refractive index and Δn is the refractive index variation.

III. EXPERIMENTAL WORK

For waveguide generation and μ-Raman measurements, a Nd:Mg:$LiNbO_3$ x-cut sample was used. The sample Nd- and Mg-doping ratios were 0.3% and 5%, respectively.

A. Waveguide generation

To generate the structural change that forms the waveguides, 796 nm Ti: Sapphire amplified laser pulses, with a pulse duration of 120 fs, a repetition rate of 1 kHz, and a 1 μJ pulse energy were used. The laser was focused inside the bulk sample by using a 10 X (NA = 0.3) microscope objective. The sample was moved along the y-direction with a 0.2 μm resolution positioning system at a rate of 50 μm/s.[34,52] The resulting structure allowed light guidance. Figure 1(a) shows the fundamental guided mode at 532 nm. In the dark elliptical areas, a refractive index decrease of 10^{-2} was estimated, while around the "ellipses" an increase of the refractive index allowed light guidance as is shown in this figure. Also, a scheme of sample processing is presented in Figure 1(b).

B. μ-Raman spectroscopy

Back-scattering μ-Raman spectroscopy in an x(zz)x configuration was used to study the residual mechanical deformations of the sample in the waveguide zone. For μ-Raman experiments, a 200 mW argon laser centered at 488 nm, and a Confocal Olympus BX-41 microscope, were used. In the latter, an objective of 50 X (NA = 0.75), a set of notch filters, and a polarizer were used.[52] The focus of the pumping laser was moved by means of a 0.1 μm resolution motorized XYZ station with steps of 0.5 μm. The Raman spectra were measured and stored for each point along the path b′b″ shown in Figure 1(a). A typical Raman spectrum corresponding to $LiNbO_3$ crystals can be observed in Figure 2. In this figure, the four $LiNbO_3$ transverse optical phonons corresponding to the configuration we used are shown. Fitting the phonons with Lorentzian functions for each point along the b′b″ path, as is shown in Figure 2, the energy shift of each $A_1(TO)_i$ phonon along b′b″ was obtained.[33,52]

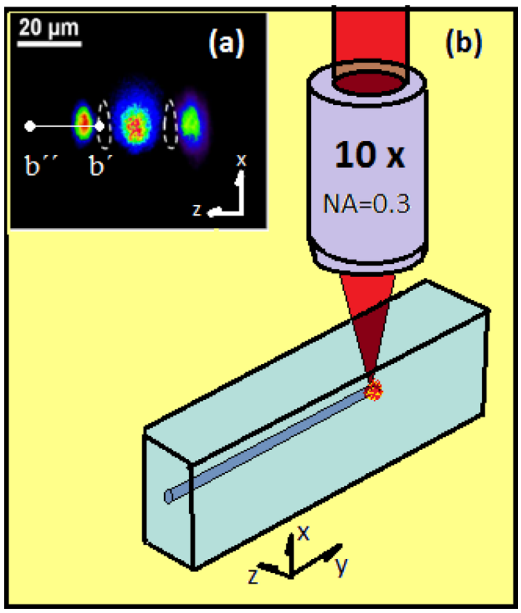

FIG. 1. (a) Guided modes. (b) Waveguide generation scheme.

C. μ-Raman energy variation analysis using a numerical simulation and phonons energy variation under hydrostatic pressure

1. Method description

The aim of this work is to present a method which can be used to estimate:

- Residual strain field after femtosecond laser processing, and waveguide refractive index field;
- Geometrical parameters of volume change during "micro-expansion" inside the material after femtosecond interaction; and

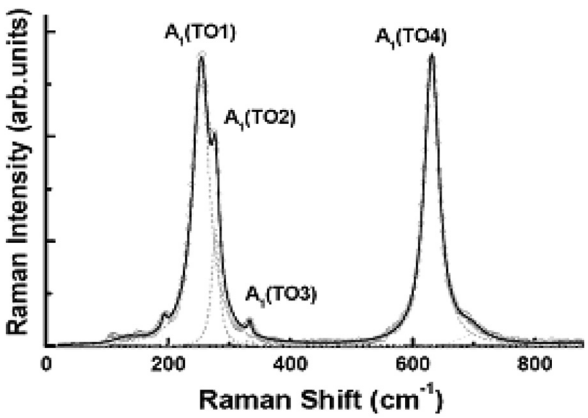

FIG. 2. Fitted μ-Raman spectra obtained in the x(zz)x configuration for a Nd:Mg:$LiNbO_3$ sample.

Downloaded 21 Dec 2012 to 163.10.0.68. Redistribution subject to AIP license or copyright; see http://jap.aip.org/about/rights_and_permissions

- Piezo-spectroscopic constants of Nd:Mg:$LiNbO_3$ lithium niobate $A_1(TO)_i$ phonons, which determine the energy shift of these phonons as a function of a strain tensor.[29–31]

This method involves the linking of three elements by the linear deformation potential theory. These elements are:

(i) the measurement of displacements of the modes $A_1(TO)$ produced in a straight waveguide generated by femtosecond laser pulses;
(ii) a finite element model similar to that implemented in other works;[42–44] and
(iii) experimental measurements[37,38] of $A_1(TO)_i$ phonons shifting under hydrostatic pressure.

For a better understanding, a block diagram of the method is shown in Figure 3.

As indicated above, deformation potential theory relates Raman phonon energy shifts to the applied strain[30,32] through Eq. (4), so, knowing the phonon energy shifts and the deformation potential constants, the strain field can be determined.

In the present analysis, the phonon energy shift in the waveguide section was measured along the b′b″ path (Sec. III B), but the $LiNbO_3$ deformation potential constants were not known beforehand. Bearing this in mind, an iterative process was generated using a finite element model. In this model an ellipse expanded, arbitrarily following Eq. (11), in an anisotropic elastic medium with the elastic properties of $LiNbO_3$.

The iterative process ended when the estimated values of dω/dp matched the values reported in the literature.[37,38]

Taking into account the fact that the residual strain field generated by the micro-explosion after the femtosecond laser interaction is the most important contribution to the light confinement,[42,43] the refractive index variation was estimated using the Mg:$LiNbO_3$ piezo-optical matrix from the resulting strain field.

2. Method procedure

(i) The initial expansion parameters mentioned in Sec. II D 1 e and the initial geometrical radii ($\boldsymbol{a} = 1\ \mu$m and $\boldsymbol{b} = 11\ \mu$m) of the ellipse shown in Figure 4 below were set.
(ii) Using these parameter values, a strain field in the *zx*-plane around the ellipse was estimated using the code MATFESA.[46]
(iii) The estimated values for z-strain and x-strain along the path b′b″ were taken from the strain field.
(iv) Then, using the strains along the path b′b″, experimental measurements of phonon energy shifts along the path b′b″, and the e' and f' values of Eqs. (4)–(8) were estimated for each phonon. To fit μ-Raman experimental measurements to the estimated strains, the minimum square error method was applied.
(v) $d\omega/dp_i$ values were estimated with Eq. (9) using the e' and f' values previously determined.
(vi) Estimated values of $d\omega/dp_1$ and $d\omega/dp_4$ were compared with the experimentally measured values ($d\omega/dp_1 = 0.2$ and $d\omega/dp_4 = 0.15$)[37,38] for each iteration j, using

$$\Delta d\omega dp_j(a_j, b_j, \alpha_{ij}, \beta_{ij}) = \sqrt{\left(d\omega/dp_{1j}(a_j, b_j, \alpha_{ij}, \beta_{ij}) - 0.2\right)^2 + \left(d\omega/dp_{4j}(a, b, \alpha_i, \beta_i) - 0.15\right)^2}, \tag{13}$$

where $d\omega/dp_{kj}(a_j,b_j,\alpha_{ij},\beta_{ij})$ is the j-iteration $d\omega/dp_k$ value.
(vii) The algorithm "fminsearch.m," available in the MATLAB standard package, was used to fit the parameters a, b, α_i, and β_i in order to satisfy the conditions in the following equation:

$$\Delta d\omega dp_j(a, b, \alpha_i, \beta_i) < 0.02. \tag{14}$$

(viii) The refractive index variation along the path b′b″ was estimated using the resulting strains, the Mg:$LiNbO_3$ piezo-optic matrix[47] and Eq. (15),[53]

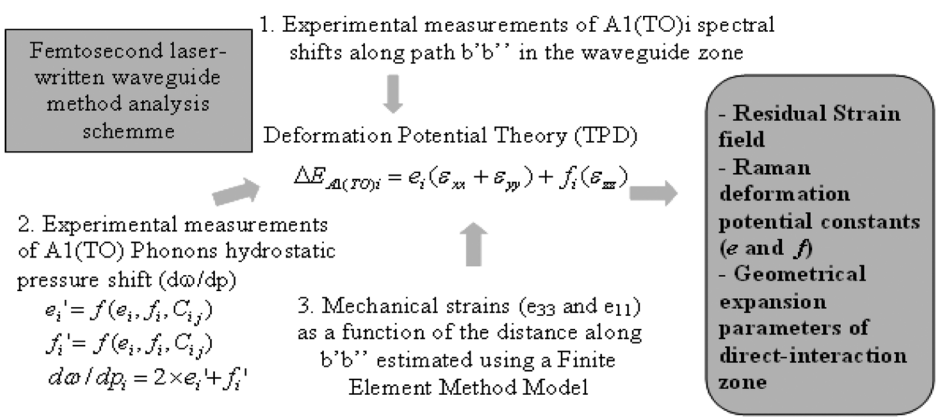

FIG. 3. Method scheme.

Downloaded 21 Dec 2012 to 163.10.0.68. Redistribution subject to AIP license or copyright; see http://jap.aip.org/about/rights_and_permissions

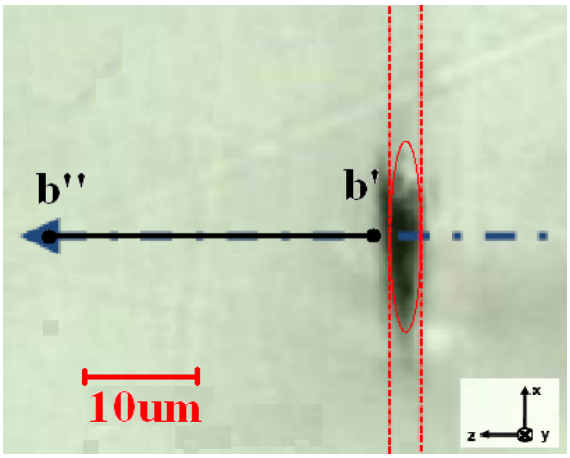

FIG. 4. Femtosecond laser modification optical image and ellipse initial geometry.

$$\Delta n_{ij} = -\frac{1}{2} \cdot n_{ii}{}^3 \sum_{kl} p_{ijkl} \cdot \varepsilon_{kl}, \tag{15}$$

where p_{ijkl} is the Mg:$LiNbO_3$ piezo-optical tensor, and ε_{kl} is the strain tensor.

IV. RESULTS AND DISCUSSION

A. Estimated strain and refractive index variation (Δn)

The strain field obtained in the present work agreed qualitatively with that obtained by other authors.[42,44] The strain values obtained along the path b′b″ are shown in Figure 5. The curve corresponding to ε_{zz} had a higher absolute value than that corresponding to ε_{xx}. The first function reached a maximum value of 0.02, while the latter reached a minimum value of −0.01. The values mentioned here were both reached at about 2 μm from the center of the modification zone. The stress range corresponding to the strains along the path b′b″ was between 0 and 4000 MPa.

The resulting refractive index also agreed qualitatively with that obtained before.[42,44] The refractive index variation obtained along the path b′b″ is shown in Figure 6. As can be seen, Δn_z and Δn_x had a maximum absolute value of 10^{-2}, situated around 2 μm from the center of the ellipse. Δn_x determined the guided zone around the ellipse. The guided zone was extended about 10 μm towards both sides of the ellipse. The refractive index variation values and stress values obtained exceeded those measured in other works[42] by an order of magnitude. This fact is attributed to a higher femtosecond pulse intensity being used during the femtosecond material processing in the present work, which means that higher residual deformations and refractive index variations are expected.[16]

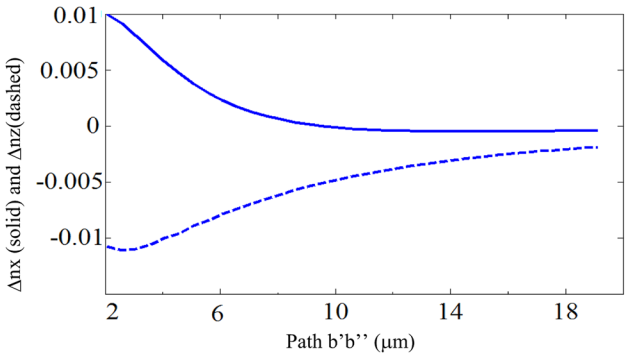

FIG. 6. Refractive index variation along path b′b″.

B. $A_1(TO)_i$ phonon shifts fitted along path b′b″

$A_1(TO)_i$ phonon energy shifts along the path b′b″ are shown in Figure 7. It can be seen that a relatively good fit of energy shifts was generated with the method developed in the current work, because the fitting curves have a mean square error of about 0.1.

In Figure 7, it can be seen that the $A_1(TO)_2$ and $A_1(TO)_3$ phonons were approximately three times more sensitive to deformations than the $A_1(TO)_1$ and $A_1(TO)_4$ phonons for the analyzed strain field. The variation of the $A_1(TO)_2$ and $A_1(TO)_3$ phonons had a similar shape although they were associated with different lattice motions.[52] The same fact occurred with the $A_1(TO)_1$ and $A_1(TO)_4$ phonons.

It can be noted that the behavior of the $A_1(TO)i$ phonons mentioned in the previous paragraph also occurred with the experimental dw/dp_i values of pure lithium niobate.[37,38]

C. Expansion parameters

The expansion parameters obtained (see Table I) indicate that, according to the model used in this work, the change in the area of the ellipse occurs mainly along the vertical direction (which corresponds to the crystal x-axis). From Table I, it can also be seen that the fit is two orders of magnitude less sensitive to horizontal expansion than to

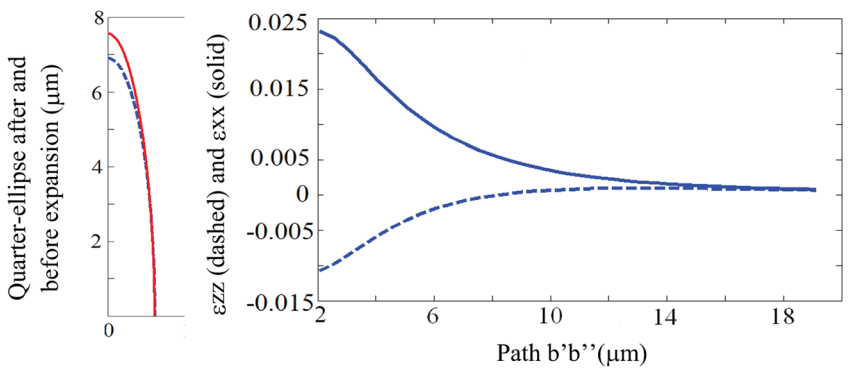

FIG. 5. Ellipse deformation (left); z-strain shown by dotted line and x-strain by solid line along path b′b″ (right).

Downloaded 21 Dec 2012 to 163.10.0.68. Redistribution subject to AIP license or copyright; see http://jap.aip.org/about/rights_and_permissions

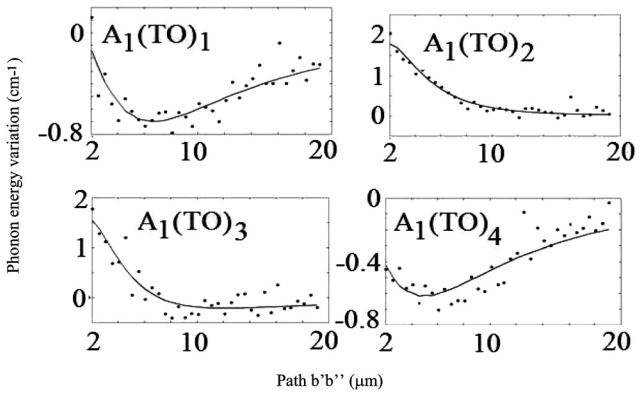

FIG. 7. Experimental measurements of $A_1(TO)_i$ spectral shifts along path b′b″ (circles) and numerical results (solid line).

TABLE I. Geometrical and expansion parameters of the ellipse.

Parameter	Value
α_1	0 ± 0.01
α_2	0 ± 0.02
α_3	0 ± 0.04
β_1	0 ± 0.003
β_2	$5 \times 10^{-3} \pm 0.5 \times 10^{-3}$
β_3	$3.1 \times 10^{-3} \pm 0.6 \times 10^{-3}$
a	$0.6 \pm 0.2\ \mu$m
b	$7.8 \pm 0.2\ \mu$m

vertical expansion. This feature was well-fitted with the trial functions proposed in this work. This result can be seen in Figure 4 (left), where a quarter of the ellipse and its expansion were plotted.

According to those values, an expansion of about 15% was reached by the ellipse after laser processing with the experimental parameters used in this paper. This value agrees with the expansion value after femtosecond laser interaction which was theoretically estimated in another work.[50]

D. Deformation potential constants or piezo-spectroscopic constants

The Mg:$LiNbO_3$ deformation potential constants shown in Table II were estimated in the current work. By taking into account the fitting parameters and their accuracy, shown in Table I, we can assert that the values of the piezo-spectroscopic constants are insensitive to horizontal expansion, within the accuracy of Table I. On the other hand, considering the horizontal and vertical expansion, the piezo-spectroscopic constant values obtained yielded a maximum error of 10%. Finally, as no previous values were found, we cannot make any comparison, but the values found are in the same range as those reported in other crystals.[33,54]

TABLE II. Deformation potential constants (cm^{-1}).

	ATO1	ATO2	ATO3	ATO4
e	-250 ± 20	-60 ± 10	-160 ± 15	-158 ± 15
f	-130 ± 10	55 ± 5	-30 ± 15	-101 ± 10

It may be noted that the e and f values obtained, except f_{A1TO2}, are all negative. This agrees with the common phonon behavior of moving to lower energies when external pressure is increased.[31,37,38]

V. CONCLUSIONS

An iterative numerical method to estimate the residual strain field in femtosecond laser written waveguides and $LiNbO_3$ $A_1(TO)_i$ Raman piezo-spectroscopic constants (e and f) is presented in this work.

This method can be used in any other transparent materials, if the values of $d\omega/dp_i$ are known or have been previously estimated. However, in order to use this method with another material, a crystal geometry and an optical phonon analysis are required.

The strain field and refractive index variations obtained in the waveguide zone are qualitatively in agreement with those presented in the literature, which should prove to be useful for improving the design and development of photonic circuits generated with femtosecond laser pulses. The proposed method can be used to characterize 3-dimensional femtosecond waveguide structures quantitatively.

Furthermore, after femtosecond laser interaction, an expansion of about 15% of the volume in the directly modified zone was estimated. This information is important for understanding the basic aspects of the femtosecond laser-material interaction.

ACKNOWLEDGMENTS

M. R. Tejerina wants to thank Eng. Francisco Bissio (Departamento de Construcciones-Facutad de Ingeniería-Universidad Nacional de La Plata-Argentina) for his valuable advice on meshing and programming the Finite Element Method. This work was partially supported by Agencia Nacional de Promoción Científica y Tecnólogica (Argentina) under project PICT-2010-2575 and CONICET (Argentina) under project PIP 0394.

[1]C. Schaffer, Ph.D. dissertation, Harvard University, Cambridge, Massachusetts, 2011.
[2]R. Gattas, Ph.D. dissertation, Harvard University, Cambridge, Massachusetts, 2006.
[3]W. Yang. Ph.D. dissertation, University of Southampton, Southampton, 2008.
[4]M. Ams, G. D. Marshall, D. J. Spence, and M. J. Withford, Opt. Express. **13**, 5676 (2005).
[5]M. Richardson, A. Zoubir, C. Rivero, C. Lopez, L. Petit, and K. Richardson, in *Micromachining Technology for Micro-Optics and Nano-Optics II: Proceedings of SPIE, Bellingham, WA (USA) 2004*, edited by E. G. Johnson and G. P. Nordin (2004), Vol. 5347, pp. 18–27. doi:10.1117/12.538386.
[6]D. Y. Liu, Y. Li, Y. P. Dou, H. C. Guo, and Q. H. Gong, Chin. Phys. Lett. **25**, 2500 (2008).
[7]J. Burghoff, C. Grebing, S. Nolte, and A. Tunnermann, Appl. Surf. Sci. **253**, 7899 (2007).
[8]S. Z. Xu, T. Q. Jia, H. Y. Sun, X. X. Li, Z. G. Cheng, D. H. Feng, C. B. Li, and Z. Z. Xu, Acta Phys. Sin. **09**, 4150 (2005).
[9]C. B. Schaffer, E. N. Glezer, N. Nishimura, and E. Mazur, in *Photonics West: Proceedings of SPIE, San Jose, CA(USA), 24–30 January 1998*, edited by M. K. Reed (1998), Vol. 3269, pp. 36–43. doi:10.1117/12.312339.

Downloaded 21 Dec 2012 to 163.10.0.68. Redistribution subject to AIP license or copyright; see http://jap.aip.org/about/rights_and_permissions

[10]A. Vailionis, E. Gamaly, V. Mizeikis, W. Yang, A. Rode, and S. Juodkazis, in *Lasers and Electro-Optics Europe (CLEO EUROPE/EQEC) Conference on and 12th European Quantum Electronics Conference, Munich, 22–26, May 2011* (IEEE, 2011).
[11]V. Mizeikisa, S. Kimurab, N. Surovtsevd, V. Jarutise, A. Saitof, H. Misawaa, and S. Juodkazisa, Appl. Surf. Sci. **255**, 9745 (2009).
[12]D. Wang, C. Li, L. Luo, H. Yang, and Q. Gong, Chin. Phys. Lett. **18**, 65 (2001).
[13]Y. Cheng, K. Sugioka, M. Masuda, K. Toyoda, M. Kawachi, K. Shihoyama, and K. Midorikawa, RIKEN Rev. **50**, 101 (2003).
[14]Y. Bellouard and M. Hongler. Opt. Express **19**, 6807 (2011).
[15]C. Schaffer, N. Nishimura, E. Glezer, A. Kim, and E. Mazur, Opt. Express **10**, 196 (2002).
[16]H. Misawa and S. Juodkazis, *3D Laser Microfabrication: Principles and Applications* (Wiley-VCH, Weinheim, 2006).
[17]J. W. Chan, T. Huser, S. Risbud, and D. M. Krol, Opt. Lett. **26**(21), 1726 (2001).
[18]E. N. Glezer and E. Mazur, Appl. Phys. Lett. **71**, 882 (1997).
[19]M. Sakakura, M. Terazima, Y. Shimotsuma, K. Miura, and K. Hirao, Opt. Express **15**, 5674 (2007).
[20]S. Juodkazis, S. Kohara, Y. Ohishi, N. Hirao, A. Vailionis, V. Mizeikis, A. Saito, and A. Rode, J. Opt. **12**, 124007 (2010).
[21]E. Anastassakis, Y. S. Raptis, M. Hunnerman, W. Ritcher, and M. Cardona, Phys. Rev. B **38**, 7702 (1988).
[22]P. Lefebvre, B. Gill, and H. Mathieu, Phys. Rev. B **40**, 7802 (1989).
[23]G. H. Loechelta, N. G. Cave, and J. Menéndez, J. Appl. Phys. **86**, 6164 (1999).
[24]G. de Portu, S. Buenob, L. Micele, C. Baudin, and G. Pezzotti, J. Eur. Ceram. Soc. **26**, 2699 (2006).
[25]J. Serrano, M. Cardona, T. M. Ritter, B. A. Weinstein, A. Rubio, and C. T. Lin, Phys. Rev. B **66**, 245202 (2002).
[26]P. Borowicza, L. Borowicza, and D. Brzezinska, in *III National Conference on Nanotechnology NANO Proceedings, Warsaw, Poland, June 22–26, 2009*; Acta Phys. Pol. A **119**, s-42- (2009).
[27]S. J. Harris, A. O'Neill, J. Boileau, W. Donlon, and X. Su, Acta Mater. **55**, 1681 (2007).
[28]R. J. Briggs and A. K. Ramdas, Phys. Rev. B Solid State **13**, 5518 (1976).
[29]S J. Harris, A. E. O'Neill, W. Yang, P. Gustafson, J. Boileau, W. H. Weber, B. Majumdar, and S. Ghosh, J. Appl. Phys. **96**, 7195 (2004).
[30]G. Irmer, T. Brumme, M. Herms, T. Wernicke, M. Kneissl, and M. Weyers, J. Mater. Sci.: Mater. Electron. **19**, 51 (2008).
[31]F. Cardeira, C. J. Buchenauer, F. D. Pollak, and M. Cardona, Phys. Rev. B **5**, 580 (1972).
[32]J. M. Wagnera and F. Bechstedt, Appl. Phys. Lett. **77**, 346 (2000).
[33]V. J. Tekkipe, A. K. Ramdas, and S. Rodrıguez Phys. Lett. A **35**, 143 (1971).
[34]A. Ródenas, L. M. Maestro, M. O. Ramírez, G. A. Torchia, L. Rosso, F. Chen, and D. Jaque J. Appl. Phys. **106**, 013110 (2009).
[35]S. Y. Wang, S. K. Sharma, and T. F. Cooney, Am. Mineral. **78**, 469 (1993).
[36]S. Y. Wang, B. L. Cheng, Can Wang, S. Y. Dai, K. J. Jin, Y. L. Zhou, H. B. Lu, Z. H. Chen, and G. Z. Yang, J. Appl. Phys. **99**, 013504 (2006).
[37]A. Jayaraman and A. A. Ballman, J. Appl. Phys. **60**, 1208 (1986).
[38]M. Filho, V. Lemos, and F. Cerdeira, J. Raman Spectrosc. **15**, 367 (1984).
[39]R. Mouras, M. D. Fontana, P. Bourson, and A. V. Postnikov, J. Phys.: Condens. Matter **12**, 5053 (2000).
[40]R. Quispe-Siccha, E. V. Mejia-Uriarte, M. Villagrán-Muniz, D. Jaque, J. García Solé, F. Jaque, R. Y. Sato-Berrú, E. Camarillo, J. Hernández, and H. Murrieta, J. Phys.: Condens. Matter **21**, 145401 (2009).
[41]K. Lengyel, L. Kovacs, A. Peter, K. Polgar, G. Corradi, and P. Bourson, Phys. Status Solidi **4**, 847 (2007).
[42]J. Burghoff, S. Nolte, and A. Tünnermann, Appl. Phys. A **89**, 127 (2007).
[43]S. Nolte, J. Burghoff, M. Will, and A. Tünnermann, in *Commercial and Biomedical Applications of Ultrafast Lasers IV Proceedings, San Jose, CA (USA), 27–29 January 2004*, edited by J. Neev, C. B. Schaffer, and A. Ostendorf (SPIE, 2004), Vol. 5340, pp. 164–171.
[44]M. Will, J. Burghoff, S. Nolte, and A. Tünnermann, in *Commercial and Biomedical Applications of Ultrafast Lasers IV Proceedings, San Jose, CA (USA), 24–27 January 2005*, edited by J. Neev, C. B. Schaffer, A. Ostendorf, and S. Nolte (SPIE, 2005), Vol. 5714, pp. 261–270.
[45]T. C. T. Ting, *Anisotropic Elasticity. Theory and Applications* (Oxford University Press, Oxford, 1996).
[46]M. Tejerina and G. A. Torchia, Appl. Phys. (2012), (in press).
[47]A. Andrushchak, B. Mytsyk, H. Laba, O. Yurkevych, I. Solskii, A. Kityk, and B. Sahraoui, J. Appl. Phys. **106**, 073510 (2009).
[48]J. Kushibiki, T. Kobayashi, H. Ishiji, and N. Chubachi, Appl. Phys. Lett. **61**, 2164 (1992).
[49]J. Kushibiki, T. Kobayashi, H. Ishiji, and C. K. Jen, J. Appl. Phys. **85**, 7863 (1999).
[50]M. Sokhna, Ph.D. dissertation, University of Kassel, Hessen, 2009.
[51]C. Gerthsen, *Physik*, 8th ed. (Springer, Berlin, 1964).
[52]A. Ródenas, Ph.D. dissertation, Universidad Autónoma de Madrid, Madrid, 2009.
[53]R. S. Weis and T. K. Gaylord, Appl. Phys. A **37**, 191 (1985).
[54]T. Miyatake and G. Pezzotti, J. Appl. Phys. **110**, 093511 (2011).

Downloaded 21 Dec 2012 to 163.10.0.68. Redistribution subject to AIP license or copyright; see http://jap.aip.org/about/rights_and_permissions